Fall Risk Assessment for the Elderly Based on Weak Foot Features of Wearable Plantar Pressure

Zhen Song, Jianlin Ou, Lin Shu, *Member, IEEE*, Guohua Hu, Shibin Wu, Xiangmin Xu, *Senior Member, IEEE*, and Zhuoming Chen

***Abstract*— The high fall rate of the elderly brings enormous challenges to families and the medical system; therefore, early risk assessment and intervention are quite necessary. Compared to other sensor-based technologies, in-shoe plantar pressure sensors, effectiveness and low obtrusiveness are widely used for long-term fall risk assessments because of their portability. While frequently-used bipedal center-of-pressure (COP) features are derived from a pressure sensing platform, they are not suitable for the shoe system or pressure insole owing to the lack of relative position information. Therefore, in this study, a definition of "weak foot" was proposed to solve the sensitivity problem of single foot features and facilitate the extraction of temporal consistency related features. Forty-four multi-dimensional weak foot features based on single foot COP were correspondingly extracted; notably, the relationship between the fall risk and temporal inconsistency in the weak foot were discussed in this study, and probability distribution method was used to analyze the symmetry and temporal consistency of gait lines. Though experiments, foot pressure data were collected from 48 subjects with 24 high risk (HR) and 24 low risk (LR) ones obtained by the smart footwear system. The final models with 87.5% accuracy and 100% sensitivity on test data outperformed the base line models using bipedal COP. The results and feature space shown the novel features of wearable plantar pressure could comprehensively evaluate the difference between HR and LR groups. Our fall risk assessment models based on these features had good generalization performance, and showed practicability and reliability in real-life monitoring situations.**

***Index Terms*— Single foot COP, fall risk assessment, weak foot, gait symmetry, gait temporal consistency, wearable plantar pressure, machine learning.**

Manuscript received September 19, 2021; revised March 18, 2022; accepted April 11, 2022. Date of publication April 14, 2022; date of current version April 25, 2022. This work was supported in part by the Technology Program of Guangzhou under Grant 202002030354 and Grant 202002030262, in part by the Science and Technology Project of Zhongshan under Grant 2019AG024 and Grant 2020B2053, in part by the Natural Science Foundation of Guangdong Province under Grant 2018A030310407, in part by the Guangzhou Key Laboratory of Body Data Science under Grant 201605030011, in part by the Major Science and Technology Projects in Guangdong Province under Grant 2016B010108008, and in part by the National Key Research and Development Project under Grant 2020YFC2005700. *(Zhen Song and Jianlin Ou are co-first authors.) (Corresponding author: Lin Shu.)*

Zhen Song, Lin Shu, Guohua Hu, and Shibin Wu are with the School of Future Technology, the School of Microelectronics, and the School of EIE, South China University of Technology, Guangzhou 510641, China (e-mail: shul@scut.edu.cn).

Jianlin Ou and Zhuoming Chen are with The First Affiliated Hospital of Jinan University, Guangzhou 510630, China.

Xiangmin Xu is with the School of Future Technology, the School of Microelectronics, and the School of EIE, South China University of Technology, Guangzhou 510641, China, and also with the Institute of Modern Industrial Technology of SCUT in Zhongshan, Zhongshan 528400, China.

Digital Object Identifier 10.1109/TNSRE.2022.3167473

I. Introduction

THE aging population is increasing globally, bringing along with it many challenges to the economy, health care and social relationship [1]. Older adults exhibit higher fall rates compared to middle aged individuals, which is attributed to reduced mobility and impaired balance function [1], [2]. Older adults, over the age of 65, exhibit fall rates of 30% to 40% [3]. The falls bring high medical costs to families and exact a huge burden on medical systems [4]. It is therefore necessary to preemptively track and intervene on behalf of people with high fall risks.

As commented by Sun and Sosnoff *et al.* [5], several traditional methods have been commonly used to assess elderly fall risk, including clinical observations and proven clinical tools, such as Berg Balance Scale (BBS), Timed Up and Go Test, etc [5]. However, there are some disadvantages of traditional clinical assessment methods, such as lack of objective measures, low cost-efficient, and restriction of poor mobility among elderly group; therefore, an objective, effective, low-cost, and user-friendly fall risk assessment method is of immense significance to medical institutions. Several sensor-based fall risk testing (SFRT) [6] technologies have showed potential for analyzing the movement and fall risk of elderly people, such as inertial sensors, and pressure sensing platform (static: pressure pad, locomotive: instrumented treadmill or low-cost pressure insole). These technologies could provide a wide range of gait and posture information [6], and exhibit adequate performance in predicting prospective fall occurrence in elderly people[7], [8], which would be a better alternative to clinical methods in fall risk assessments. Compared to other technologies, the shoe system with plantar pressure sensors have been more suitable for long-term monitoring because of its low obtrusiveness [9] and portability. This study implemented the shoe system with plantar pressure sensors for the elderly fall risk assessment as the shoes represented ordinary shoes without any impediment to daily life [10].

Furthermore, the battery supported 20 hours of continuous real-time monitoring and the shoes were equipped with low-cost and high durability pressure sensors.

The center-of-pressure (COP) is the point representing a weighted average of all vertical ground reaction forces (VGRF) over the surface. COP methods have been used in studies on balance-related problems and posture control, such as the well-known inverted pendulum model [11], extrapolated center of mass [12], and COP threshold boundary [13]. Several investigations concluded that the bipedal COP during quiet stance was sensitive to postural performance [14], [15]. Bipedal COP features from data recorded by a force platform were applied to study the risk of falling and static postural balance [16]–[18]. In motion analysis, a unique dynamic COP trajectory evaluated by instrumented treadmill, the "Pedotti" diagram, also known as "butterfly" diagram, reflected the specific variability of COP in some patients with neurological diseases, such as Parkinson's disease and Multiple sclerosis [19], [20].

In the above bipedal COP methods, being static and locomotive were inconvenient for migration to a shoe system or other devices with pressure insole due to the lack of relative position information; hence, it was impossible to strictly apply them in daily life for long-term monitoring. There have also been studies attempting to fix both feet in a virtual plane to calculate the "butterfly" diagram [21], [22], although this might introduce more errors and lack of interpretability compared with the real plane. As a part of the "butterfly" diagram single foot COP trajectory, the gait line (GL) also reflected the stability and regularity of the foot's heel-to-toe movement [22] and was easy to migrate owing to the unuse of relative positions.

This study aimed at assessing the fall risk among elderly people based on multi-dimensional features extracted from GLs. A definition of "weak foot", i.e., one weaker side foot that has partially lost the integrity and regularity of gait, and its discriminant method are proposed to eliminate the misleading effect on classification due to the sensitivity of single foot features, leading to a poor performance in fall risk assessments. Analysis of movement symmetry had already been a pervasive and practical way to evaluate the balance and postural regulation of people [23]–[25]; however, gait variety in time sequence were seldom adopted, which may reflect gait fatigue [26] and other factors in high risk population. We, therefore, extract some gait symmetry related and sequential consistency-related features based on "weak foot" to assist fall risk assessments. Seven traditional machine learning classifiers are employed as candidates in our study, namely logistic regression (LogiR), k-Nearest neighbor (KNN), support vector machine (SVM), decision tree (DT), random forest (RF), gradient boosting decision tree (GBDT) and AdaBoost.

II. Methods

A. Data Collection

48 adults aged 65 and older who could walk for two minutes independently were recruited for this study. All subjects were recruited from inpatients in the Rehabilitation Department of the First Affiliated Hospital of Jinan University. Before the data collection, all subjects were required to perform BBS test and fill out a questionnaire, including basic characteristics, exercise habit, fall and rehabilitation history, shoe wearing habits, and medication. All experimental procedures were approved by IRB of the First Affiliated Hospital of Jinan University (KY-2020-087) on December 24, 2020.

TABLE I
SUBJECT CHARACTERISTICS

	Gender (M/F)	Age (years)	BMI (Kg/m^2)
Low risk (BBS $\geq$ 40)	10/14	72.3±6.0	23.5±2.9
High risk (BBS$<$40)	15/9	75.9±6.9	23.5±2.8

BBS: Berg balance scale.

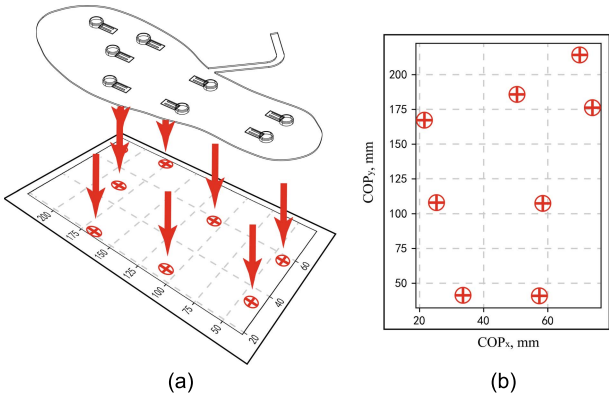

Fig. 1. Sensor position. (a) Pressure insole and sensors in shoe system. (b) Distribution of 8 pressure sensors on the insole. x- and y-axes represent medial-lateral and anterior-posterior direction respectively.

Subjects were identified as high risk (HR) of fall if their BBS score was less than 40 [27] or low risk (LR) of fall if otherwise. The characteristics of the subjects such as gender, age, and BMI, are shown in Table I. There are no significant differences in age ($p = 0.068$) and BMI ($p = 0.984$) between the HR and LR groups as evaluated by the t-test.

A prepared intelligent footwear system [10] was used to collect plantar pressure data. As can be seen in Fig. 1 (a), in the sensing insole of shoe system, eight pressure sensors are distributed in different positions of the insole beneath each foot. As shown in Fig. 1 (b), the sensor coordinates of different shoe sizes are scaled to a unified coordinate system in the subsequent data processing.

Walking experiment was divided into preparation and formal stages. In preparation stage, the subjects wore the shoe system for simple activities to ensure that the shoes were of proper size and their feet would not slip during walking. The main purpose of this stage is to make the subjects familiar with this pair of shoes and be able to walk naturally without affecting the natural gait. As shown in In Fig. 2, in formal walking stage, the subjects were asked to walk the 20-meter-long corridor for over two minutes. They were followed by medical staff at a distance to ensure safety of elderly subjects and supervise them to walk at a normal speed and gait with arm swing. Arm swing could influence gait parameters [28], [29]

Fig. 2. Walking experiment. (a) Data collection. (b) Walking under the supervision of medical staff. The red box on the left shows the plantar pressure collection software on the mobile phone.

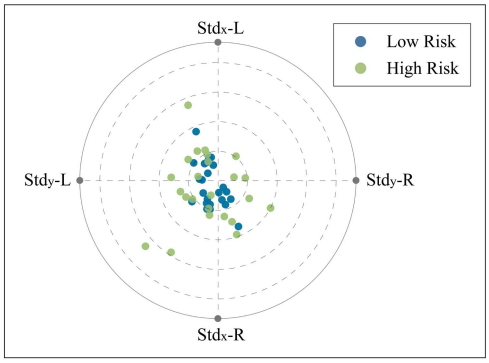

Fig. 3. RadViz for four features.

and needs to be controlled in balance-related work. Plantar pressure data were collected at 20 Hz and uploaded to a mobile phone in real time.

B. Feature Extraction

The features extracted in this section focus on multi-dimensional analysis on single foot COP obtained by the wearable plantar pressure measurement shoe system. Before the feature selection, the pressure time series of each subject was divided into single gait cycle by identifying minimum total VGRF value from all eight sensors. To reduce the impact of gait start-up, the first two steps of each subject were discarded, and the first 90 gait cycles in remaining data were used.

Some bipedal features were applied in our analysis of single foot to evaluate the shape and size of GLs. The probability distribution methods were used to reflect spatial symmetry of GLs. Temporal changes of GLs were also considered, and three types of features were extracted. Three common bipedal COP features from "butterfly" diagram were also extracted and used as baseline for comparison, including lateral variability, ant-post variability, and lateral symmetry [20]. Here, COP is a kinetic parameter, which represents a weighted average of all the plantar pressures, and is used to track transfer of weight. For each foot, COP can be calculated as:

$$X = \frac{\sum_i^n F_i X_i}{\sum_i^n F_i}, Y = \frac{\sum_i^n F_i Y_i}{\sum_i^n F_i} \tag{1}$$

where n is number of pressure sensor, F_i refers to VGRF, and (X_i, Y_i) represents relative coordinates of each sensor.

Forty-four features were extracted from COP in time series, including GL, symmetry, and temporal consistency related features.

1) Raise and Definition of the "Weak Foot": RadViz [30], [31] is a visualization method that maps multi-dimensional feature space to two-dimensional space. The sample projection in two-dimensional space is obtained by opposite pulling of springs with different spring constants, which represent the features with different values. It can help us more intuitively understand the relationship between feet. As can be seen in Fig. 3, we plotted RadViz with four COP statistic parameters, including Std_y-L (Std in anterior-posterior (AP) COP trajectory of left foot), Std_y-R (Std in AP COP trajectory of right foot), Std_x-L (Std in medial-lateral (ML) COP trajectory of left foot) and Std_x-R (Std in ML COP trajectory of right foot). For people with HR in the RadViz, majorities of their distributions were in non-center position and surrounding area of LR people, meaning the asymmetry gait of HR people might be caused by one weaker side. For instance, as shown in Fig. 3, the two HR subjects in the lower left corner of the figure imply that they were closer to the side of Std_y-L because their right feet exhibit smaller COP variability in AP direction; moreover, there was a lack of stability and regularity of the foot-to-toe movement [22]. However, the weaker side was not just the same side for all HR people. There were also some HR people with weak left feet, who were closer to the side of Std_y-R in the figure. If only the single foot features were used, the special cases of these HR people were ignored. For instance, the misleading effect on classification of left foot features would lead to poor results in some cases who do not meet the condition of weaker left. The above phenomenon was defined as the "sensitivity of single foot features." According to the analysis of RadViz, the following definition and discrimination of "weak foot" was made to eliminate the misleading effect and sensitivity of single foot features.

Weak foot, i.e., one weaker side foot that has partially lost the integrity and regularity of gait, can be determined by standard deviation in AP-COP trajectory. Through the discriminant (2), the weak foot has a small variability in the AP direction.

$$\begin{cases} (X^W, Y^W) = (X^L, Y^L), Std_y^L < Std_y^R \\ (X^W, Y^W) = (X^R, Y^R), Std_y^L > Std_y^R \end{cases} \tag{2}$$

where (X^L, Y^L), (X^R, Y^R), and (X^W, Y^W) are COP trajectory of left foot, right foot, and weak foot respectively.

2) Weak Foot and Single Foot GL Features: GL is the COP path calculated in one foot, which is a bivariate distribution defined by AP and ML directions. Therefore, we can extract one-dimensional (1D) features along AP and ML directions and two-dimensional (2D) features from support plane, both of which describe the size and shape of path over the support plane. For the weak foot determined by discriminant (2) of each subject, four 1D and four 2D features were calculated.

The 1D features can effectively indicate different swing and deviation along one direction between HR and LR subject. The mean value and standard deviation in both AP and ML directions can be calculated by equations (3−6), where x and y

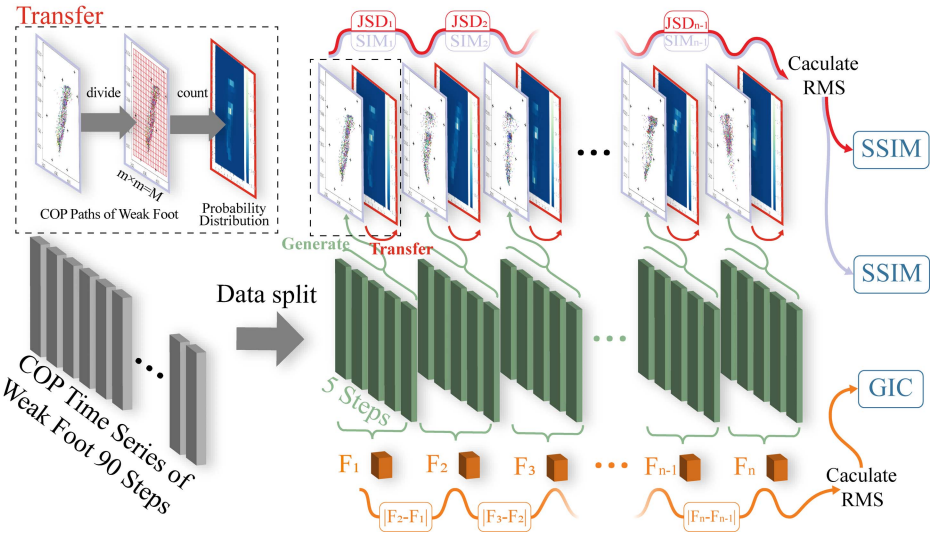

Fig. 4. Temporal consistency related features. The process in the black dotted box represents the transformation from COP paths to probability distribution. n is 90/5. M and m represent the number of blocks in probability matrix and the number of intervals respectively.

represent the ML and AP direction, respectively, W represents the weak foot, and N is the total sample number in 90 gait cycles.

$$Mean_x^W = \frac{\sum_{i=0}^{N} X_i^W}{N} \tag{3}$$

$$Std_x^W = \sqrt{\frac{\sum_{i=0}^{N} (X_i^W - \overline{X^W})^2}{N}} \tag{4}$$

$$Mean_y^W = \frac{\sum_{i=0}^{N} Y_i^W}{N} \tag{5}$$

$$Std_y^W = \sqrt{\frac{\sum_{i=0}^{N} (Y_i^W - \overline{Y^W})^2}{N}} \tag{6}$$

Similarly, the 2D features can indicate gathering and dispersing degree of GL points in HR and LR subject. For 2D feature, mean value of resultant distance (*MRD*), standard deviation of resultant distance (*SRD*), total excursions (*TOTEX*) and 95% confidence circle area (*CCA*) can be calculated by equations (7−10), where *RD* represents resultant distance and $z_{0.5}$, the 95% confidence level z statistic, is 1.645 here [32].

$$MRD^W = \frac{\sum_{i=0}^{N} \sqrt{(X_i^W - Mean_x^W)^2 + (Y_i^W - Mean_y^W)^2}}{N} \tag{7}$$

$$SRD^W = \sqrt{\frac{\sum_{i=0}^{N} (RD^W - MRD^W)^2}{N}} \tag{8}$$

$$TOTEX^W = \sum_{i=0}^{N-1} \sqrt{(X_{i+1}^W - X_i^W)^2 + (Y_{i+1}^W - Y_i^W)^2} \tag{9}$$

$$CCA^W = \pi(MRD^W + z_{0.5}\sqrt{\frac{\sum_{i=1}^{N} (RD^W)^2}{N} - (MRD^W)^2})^2 \tag{10}$$

Notably, a total of eight features are also calculated on the left and right feet respectively.

3) Symmetry Related Features: As evident from previous studies [25], [33], movement symmetry, i.e., the similarity of left and right body movements, is a vital motion feature in balance analysis, and it has become a pervasive and practical way to evaluate some diseases and postural regulation in people. Usually, a marked difference has been observed between the affected and unaffected limbs among HR people with pathological gait [33].

There have been many symmetry measures purposed in previous studies. Once we had obtained the movement data via sensors, depth sensing, video camera and others, these data could be used to evaluate the symmetry performance in certain way. However, there is no accepted standard in symmetry measurement; for example, in continuous signal, many symmetry indices have been used to measure gait symmetry, such as symmetry index, symmetry angle, gait symmetry (GA) and trend symmetry, and in "butterfly" diagram, lateral symmetry, left or right deviation of the intersection point from "zero position" is commonly used.

In order to measure gait symmetry well with single foot COP paths, traditional index *GA* was not only extracted, but the similarity (*SIM*) and JS-divergence (*JSD*) were also calculated from probability distribution of both sides. *SIM* was used to measure the similarity of the GL distribution between two feet, ranging from 0 to 1. *JSD*, also ranging from 0 to 1, was a variant based on Kullback-Leibler divergence, and a symmetric measure of the difference between probability distribution.

GA can be calculated by equation (11), where F_L and F_R represent corresponding GL features on left and right feet.

$$GA(F_L, F_R) = \left| \ln \frac{\min(F_L, F_R)}{\max(F_L, F_R)} \right| \tag{11}$$

Before the extraction of *SIM* and *JSD*, transformation from COP paths to probability distribution is needed. As can be seen in black dotted box of Fig. 4, according to the position of sensors, x and y coordinates of both sides are divided into

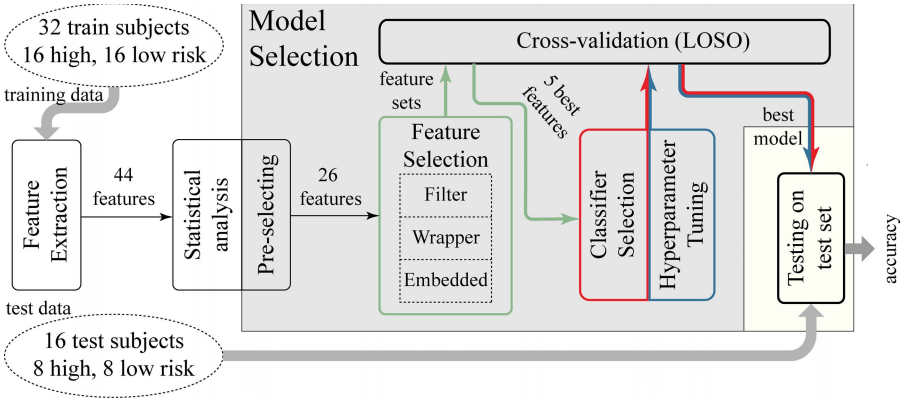

Fig. 5. Pipeline of statistical analysis and model selection.

350 intervals to obtain a 350 × 350 probability matrix. The value of the matrix elements is the number of GL points in each block divided by total number. After that, the probability matrix obtained is a 2D form of probability distribution.

Then, *SIM* and *JSD* can be calculated by equation (12) and (13), where S_L and S_R represent probability distribution of left and right foot respectively.

$$SIM = \sum \min(S_L, S_R) \tag{12}$$

$$JSD = \frac{1}{2}\sum S_L \log_2 \frac{S_L}{\frac{S_L+S_R}{2}} + \frac{1}{2}\sum S_R \log_2 \frac{S_R}{\frac{S_L+S_R}{2}} \tag{13}$$

A total of 10 features were extracted in this section.

4) Temporal Consistency Related Features: Temporal changes of gait in the weak foot were considered in this part. As shown in Fig. 4, three novel temporal consistency related features were extracted from the weak foot. The COP time series of 90 steps for the weak foot were divided into several five steps before the feature extraction.

Gait inconsistency (*GIC*), which reflects changes in the weak foot features over time, could be calculated by equation (14), using $n = 90/5$ and F as the weak foot features extracted from each divided time series.

$$GIC = \sqrt{\frac{1}{n-1}\sum_{j=1}^{n-1} \left|F_{j+1} - F_j\right|^2} \tag{14}$$

Sequential similarity (*SSIM*) and Sequential JS-divergence (*SJSD*) were proposed following the same idea as above, and could be calculated by equation (15) and (16), as shown at the bottom of the page, where M was number of blocks in probability matrix transferred from divided COP time series. Specifically, the number of intervals in the transformation process was no longer 350 because of the change in steps. To ensure that the average number of COP points in blocks remained approximately unchanged, the number of intervals should be set to 80 in the case of five steps.

A total of ten features were extracted in this section.

C. Statistical Analysis and Model Development

As reviewed by Shany *et al.* [6], many researchers were optimistic about their results on SFRT. In many cases, inflations of the accuracy occurred easily because of data leakage that were often due to an unclear and nonstandard model selection process. Specifically, pre-selecting and feature selection procedures are sometimes misused as an external process to model selection.

To avoid the above mistakes, as can be seen in Fig. 5, we clearly presented the details of statistical analysis and model selection. As suggested by Tal *et al.* [6], we used the overall method of embedding cross-validation into holdout validation. Outside of the model selection, holdout method was firstly used to divide data from 48 subjects into a test set (16 test subjects: eight HR, eight LR) and a training set (32 train subject: 16 HR, 16 LR) randomly. The test set had never been used until the best model were determined, and the data analysis and model development were performed on training set.

1) Statistical Analysis and Pre-Selecting: In statistical analysis, the Student's t test was performed on the features extracted from training data to evaluate the difference between HR and LR groups. A p-value < 0.05 was considered statistically significant, and used as a criterion of pre-selecting.

2) Feature Selection: As shown in Fig. 5, we used three types of feature selection methods to ensure that the optimal feature set not missed, including filter, wrapper, and

$$SSIM = \sqrt{\frac{1}{n-1}\sum_{j=1}^{n-1}\left(\sum_{i=1}^{M} \min(S_i^j S_i^{j+1})\right)^2} \tag{15}$$

$$SJSD = \sqrt{\frac{1}{n-1}\sum_{j=1}^{n-1}\left(\frac{1}{2}\sum_{i=1}^{M} \log_2 \frac{S_i^j}{\frac{1}{2}(S_i^j + S_i^{j+1})} + \frac{1}{2}\sum_{i=1}^{M} \log_2 \frac{S_i^{j+1}}{\frac{1}{2}(S_i^j + S_i^{j+1})}\right)^2} \tag{16}$$

embedded methods. Five filter methods were used: mutual information maximization (MIM) [34], minimal-redundancy and maximal-relevance (mRMR) [35], representative feature method [16], t-test based ranking, and model based ranking. Two wrapper methods, sequential forward selection (SFS) and sequential backward selection (SBS) were both adopted. For the embedded method, in the training of RF and DT model, the model structures were determined by observing the effect of manipulating different features on tree nodes in training, so important features were more likely to be near the root node. The feature importance could be estimated by finding the feature depth or average depth on the tree.

3) Classifier Selection and Hyperparameter Tuning: In the classifier selection, LogiR, KNN, SVM, DT, RF and AdaBoost were employed as candidates. Optuna [36], a new design-criteria optimization framework, was used to efficiently find the best hyperparameter in a large search space. We mainly explored two hyperparameters for each classifier, as follows: misclassification cost C and maximum iteration in LogiR, number of neighbors and leaf size in KNN, C and *gamma* in SVM, maximum depth and minimum samples of leaf in DT and RF, and number of estimator and learning rate in GBDT and AdaBoost.

D. Model Evaluation

The optimal model was chosen after feature selection, classifier selection, and hyperparameter tuning according to the accuracies of leave-one-subject-out (LOSO) validation inside the training data. It was finally tested on a test set, where evaluation parameters include accuracy, sensitivity, specificity, positive predictive value (PPV) and negative predictive value (NPV). Confidence interval for accuracy was also calculated by Wilson interval in Equation (17), which was vital for accuracy from small test set [7].

$$CI = \frac{P + \frac{z^2}{2N} \pm z\sqrt{\frac{P}{N} - \frac{P^2}{N} + \frac{z^2}{4N^2}}}{1 + \frac{z^2}{N}} \tag{17}$$

where P is accuracy, N is size of test set, and z is 1.96 for a 95% confidence interval [7].

III. Results and Discussions

A. Statistical and Pre-Selecting Results

As shown in Table II, the p-values of 44 features from the Student's t test were listed. Twenty-six features in total had significant differences in mean between HR and LR groups ($p < 0.05$). The results of each type of features were discussed separately as follow.

1) Statistical Results of Single and Weak Foot GL Features:

a) Effectiveness of "weak foot": To verify whether the proposed definition of "weak foot" can effectively eliminate the sensitivity of single foot features, the weak foot and single foot features were compared firstly. As can be seen in Fig. 6, two typical features in different dimensions were taken as examples here (Std in y-coordinate COP trajectory and Total excursion). Weak foot features always had higher statistical significance both in 1D ($p < 0.001$) and 2D ($p < 0.001$). However, single foot features were sensitive to side, and had lower or even no significance (Std_y^R) in one side. The statistical significance of left foot features was sometimes slightly lower than weak foot, and their values between two groups of subjects also had significant difference, from which it could be inferred that most people's weak foot was on the left, presumably because the effect of dominant limb or differences between leg roles during locomotion. Left foot features could also classify the subjects well, and played same role as the weak foot in most cases; but the simple reasons above were not all the causes of weak foot. Physical injury, such as fall and surgery, and diseases may also link with factors leading to weak foot. The randomness of these factors led to the uncertainty of the weak foot, as well as the inequivalence between weak foot and left foot. In a sense, according to the statistical results that weak foot features did perform better than single foot feature both in 1D and 2D, the proposed definition of "weak foot" and its

TABLE II
List of Features

Feature	Equation	p-value	Feature	Equation	p-value
$Mean_x^L$	(3)		$TOTEX^W$	(9)	+++
Std_x^L	(4)		CCA^W	(10)	+++
$Mean_y^L$	(5)		$GA\text{-}Mean_x$	(3), (11)	
Std_y^L	(6)	+++	$GA\text{-}Std_x$	(4), (11)	
MRD^L	(7)	+++	$GA\text{-}Mean_y$	(5), (11)	
SRD^L	(8)	+++	$GA\text{-}Std_y$	(6), (11)	+
$TOTEX^L$	(9)	+++	SIM	(12)	+
CCA^L	(10)	+++	JSD	(13)	+
$Mean_x^R$	(3)		$GA\text{-}MRD$	(7), (11)	+
Std_x^R	(4)	+	$GA\text{-}SRD$	(8), (11)	
$Mean_y^R$	(5)		$GA\text{-}TOTEX$	(9), (11)	++
Std_y^R	(6)		$GA\text{-}CCA$	(10), (11)	+
MRD^R	(7)	++	$GIC\text{-}Mean_x$	(3), (14)	
SRD^R	(8)	+	$GIC\text{-}Std_x$	(4), (14)	
$TOTEX^R$	(9)	+++	$GIC\text{-}Mean_y$	(5), (14)	+
CCA^R	(10)	+++	$GIC\text{-}Std_y$	(6), (14)	++
$Mean_x^W$	(3)		$SSIM$	(15)	
Std_x^W	(4)	+	$SJSD$	(16)	
$Mean_y^W$	(5)		$GIC\text{-}MRD$	(7), (14)	+
Std_y^W	(6)	+++	$GIC\text{-}SRD$	(8), (14)	
MRD^W	(7)	+++	$GIC\text{-}TOTEX$	(9), (14)	++
SRD^W	(8)	++	$GIC\text{-}CCA$	(10), (14)	

GA: Gait asymmetry, *GIC*: Gait inconsistency, Student's t test was applied with these data: +: p<0.050, ++: p<0.010, +++: p<0.001. The number in column "Equation" is equation number needed to calculate the corresponding feature.

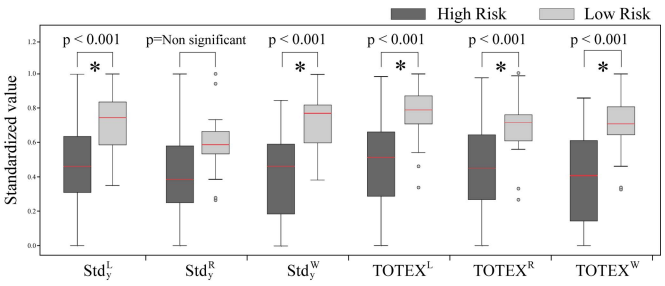

Fig. 6. Comparison between statistical results of single and weak foot features. All features were standardized. Significant difference between the two groups is denoted by *.

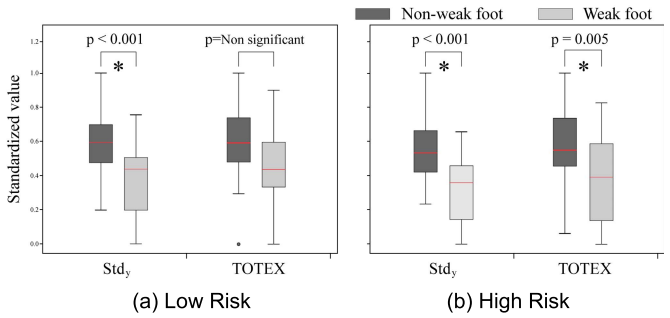

Fig. 7. Comparison between statistical results of low risk and high risk. The features extracted from non-weak side were not added to feature set.

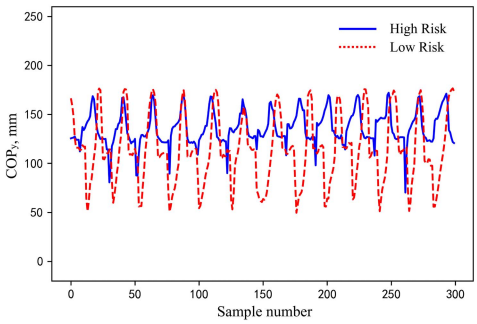

Fig. 8. COP$_y$ of weak foot in HR and LR subject. y represents AP direction respectively.

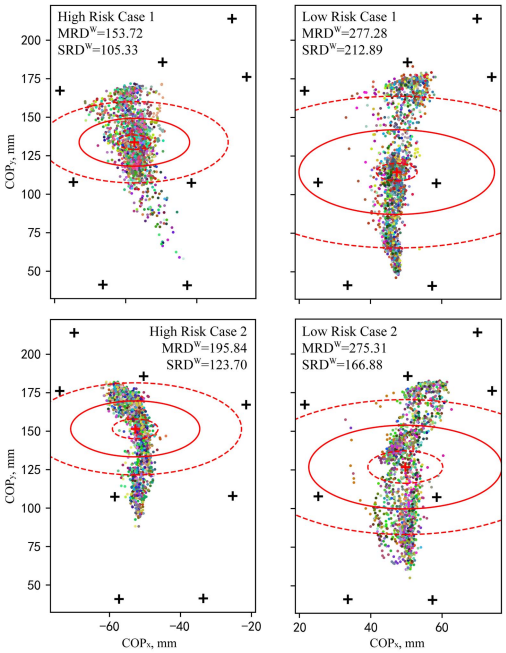

Fig. 9. COP path of weak foot in HR and LR subject. x- and y-axes represent ML and AP direction respectively. The black and red cross stand for the relative position of each sensor and (MeanW x, MeanW y) respectively. The red solid line and dotted line stand for MRD^W and SRD^W. The different colors of COPs represent gait cycles.

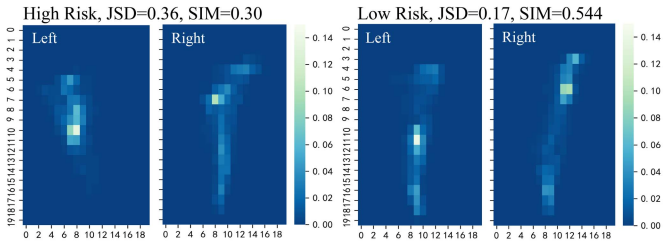

Fig. 10. Probability matrix of high risk and low risk subjects. For convenience of display, the resolution of probability matrix in the figure was 20*20, but SIM and JSD were still calculated on 350*350 probability distribution.

related features corrected the uncertainty of these factors, and the effect of sensitivity in single foot feature was eliminated.

b) Different effects of "weak foot" on HR and LR: As shown in Fig. 7, the same 1D and 2D features were extracted on both weak and non-weak sides to perform t test between two sides. In the HR group, the difference between weak foot and non-weak foot was more significant, while in the LR group, even some features were not significant, implying that weak foot phenomenon and impaired regularity of gait are more obvious among the HR group. For the LR group, because of the better symmetry between the weak and non-weak side, whichever side were determined as weak side has less effect. The misleading effect on classification that we want to eliminate by "weak foot" mainly comes from HR individuals, which can also be seen from RadViz where most of the individuals distributed around were HR.

c) Weak foot feature analysis: The loss of gait integrity and regularity was reflected by decreased variability and deviation of GL in weak foot. The abnormal phenomenon could be found in the gait of weak foot in the HR groups. As shown in Fig. 6, the values of weak foot features are generally smaller in the HR groups both in 1D and 2D. The 1D features could effectively indicate different swing and deviation along one direction between HR and LR subjects. For instance, as can be seen in Fig. 8, HR subject apparently show a smaller swing and larger deviation from the center of the y-coordinate, indicating the gait cycle from heel landing to toe off was not completed. In a normal case, like LR, the upper and lower half curves should be symmetrical; however, in the HR group, the lower half curve amplitude was smaller. This case show that HR subjects prefer to land with the entire weak foot rather than the heel. Similarly, the 2D features indicated gathering and dispersing degree of GL point. As can be seen in Fig. 9 the GLs of HR subjects were more concentrated in a certain area. The smaller red solid and dotted circles in this figure, indicating smaller MRD^W and SRD^W, also reflected the aggregation in HR subjects. The phenomenon was also common in some subjects whose weak foot was on the right side, as seen in HR case 2.

2) Statistical Results of Symmetry Related Features: For symmetry related features, *GA* applied in some certain features had good results; both *SIM* (p =0.043) and *JSD* (p = 0.038) based on probability distribution also had significant difference in mean value between two groups, which meant probability distribution could be effectively used to generalize the shape of COP paths. For instance, as shown in Fig. 10, there was an obvious difference between distribution shape and highlight

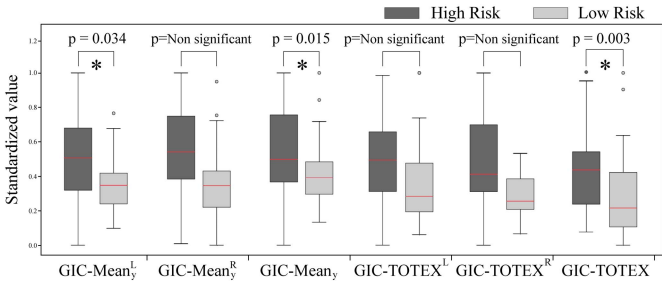

Fig. 11. Comparison between statistical results of GICs. GICs were also calculated in single foot for comparison, but not added to feature set.

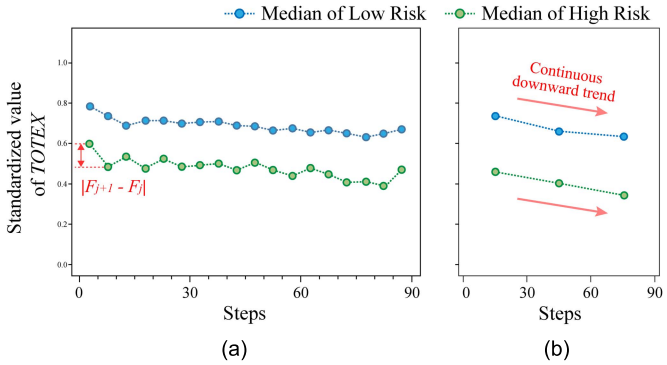

Fig. 12. TOTEX changes over time in low and high risk groups. (a) TOTEX calculated every five steps. (b) TOTEX calculated every 30 steps.

area of two sides among HR subjects, which resulted in lower *SIM* and higher *JSD* than LR.

3) Statistical Results of Temporal Consistency Related Features:

a) Feature resolution analysis: For temporal consistency features, no significance of *SSIM* ($p = 0.350$) and *SJSM* ($p = 0.200$) denoted that probability distribution might lose its effectiveness in time sequence. When 350*350 probability matrix was used to extract features, *SIM* and *JSD* had significant difference between two groups, but when the resolution was changed to 80*80 according to the number of steps, *SSIM* and *SJSD* lost their effectiveness to describe the similarity and difference. The compromise of resolution was vital for features based on probability distribution. High resolution with few samples was easy to cause a decrease in comparability. Low resolution with lots of samples led to loss of GL information. Therefore, 80*80 deduced by linear relationship between the number of blocks in probability matrix and the number of samples was not optimal resolution. The phenomenon could be explained by two possible reasons. The number of samples from 5 steps were relatively small for calculating probability distribution, on the other hand, there was no linear relationship mentioned above.

b) Necessity of extracting GICs on weak foot: Although probability distribution was more suitable for large sample analysis, and *SSIM* and *SJSD* failed to reflect temporal consistency, *GIC*, as a more direct method, well reflected the temporal variety of gait in weak side. *GIC* were extracted from weak foot COP time series, and we also extracted it from single foot for comparison. Two features in different dimensions were taken as example in Fig. 11 (*GIC* of mean in y-coordinate COP trajectory and *GIC* of the total excursion of COP trajectory). It was easy to find out temporal change of gait was more significant in the weak foot, and *GIC* was more reasonable to be applied to the weak foot for higher statistical significance in most cases ($p = 0.015$ and $p = 0.003$), which reflects that weak foot is more prone to time-related effect, and *GIC*s are indeed necessary for extraction from the weak side. During the experimental process of walking, we did find that the gait of ill or injured side changed measurably over time. Notably, *GIC-Std*$_y$ was a special case, which had the lower p-value when it was applied in right foot rather than weak foot.

c) GIC feature analysis: No matter which side or weak side the features were extracted from, the values of *GIC* were all higher in HR groups, which reflected that under some time-related effect, gaits of HR were easily affected to varying degrees, making greater changes in gait than LR at same time interval. According to equation (14), *GIC* reflects the inconsistency in time by accumulating the difference between local gait feature F_j. Therefore, to analyze the time-related effect reflected by GIC, as can be seen in Fig. 12 (a), the *TOTEX* was analyzed as F_j and calculated every five steps to simulate the extraction of *GIC-TOTEX*. The median changes of the two groups are shown in different colors. Compared with LR group, the difference between local adjacent features ($|F_{j+1}$-$F_j|$) was greater in HR group, resulting the fluctuating line and larger *GIC-TOTEX*. This local time-related effect shows that the gait of HR subjects has higher inconsistency in a short time, and is consistent with the statistical result of *GIC*.

As can be seen in Fig. 12 (b), *TOTEX* was also extracted every 30 steps to eliminate the impact of local time-related effect by expanding the extraction interval. The continuous downward trend of *TOTEX* indicated that the gait integrity of subject gradually declines over time, which might be associated with physical fatigue, because fatigue is also a gradual process and occurs in repeated or continuous muscle activation [37], such as walking test [38] and action repetition [39]. In addition, some characteristics of gait have been proved to change owing to fatigue [38]–[40], and the elderly are more prone to fatigue [41]. However, other factors may also cause this time-related effect. Further studies are needed in the future.

Features with high significance were more likely to contribute more to classification. Therefore, after statistical analysis, 26 features with significance ($p < 0.05$) were selected from raw feature set for the next step.

B. Model Selection Results

During the process of model selection, test data set was strictly guaranteed not to be used. Therefore, the final accuracy could truly evaluate the generalization performance of the model and effectiveness of model for new subject.

1) Feature Selection Result: The accuracy derived from DT with default hyperparameters was used as the evaluation parameter. From all feature selection method, a subset of five features was selected out of a total of 26 features. As shown

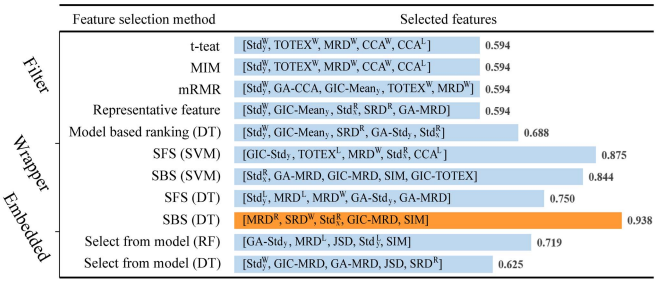

Fig. 13. Results of feature selection.

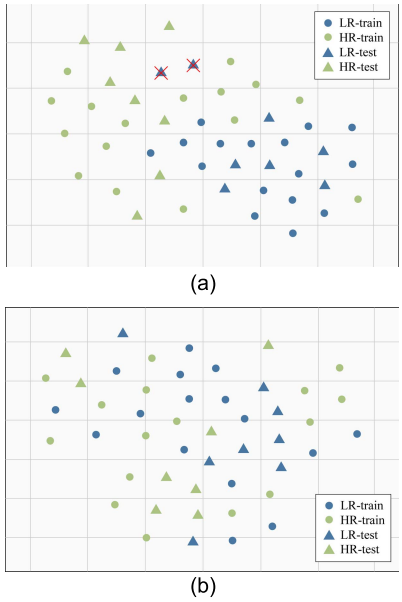

Fig. 14. Feature Space. (a) t-SNE of selected single foot features. (b) t-SNE of base line features. The red crosses in (a) represents the case who were misclassified in final test, and the rest of the test cases were classified correctly. Abbreviations: HR, high risk; LR, low risk.

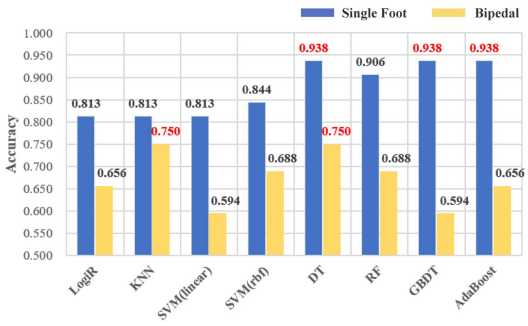

Fig. 15. Results of classifier selection and hyperparameter tuning. SVM employed both linear and rbf kernels.

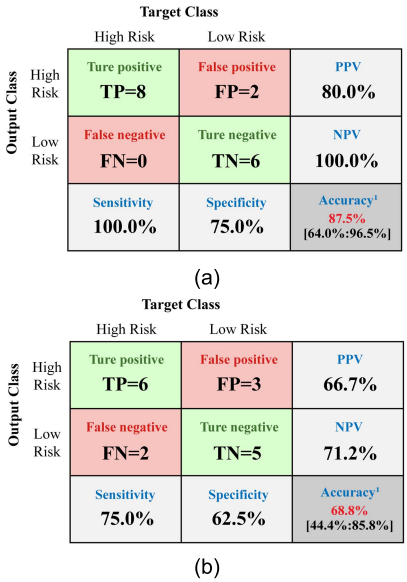

Fig. 16. Confusion matrix on test set. (a) Three optimal model (DT, GBDT, AdaBoost) with selected five features. (b) Two optimal model (KNN, DT) with base line features. [1]Accuracy [95% Confidence Interval]. Different optimal models with same features had the same results.

in Fig. 13, filter methods had a poor performance in our feature set. Especially, the t-test, MIM, and model-based ranking method were more likely to choose top features owing to the lack of consideration for redundancy and correlation between features; wrapper methods tended to choose more comprehensive feature sets covering different types of features and had better selection results. It could be seen that sequential backward selection with DT performed best, so the features selected with this approach were used in next processes, including single foot feature (MRD^R *and* Std_x^R), weak foot feature (SRD^W), symmetry related feature (*SIM*) and temporal consistency related feature (*GIC-MRD*).

t-SNE [42] were utilized to decompose five features above to three or two dimensions so that each subject can be plotted in the feature space. As shown in Fig. 14 (a), under the rules of the selected features, most of the subjects with same label tended to concentrate in certain area, and were easy to be classified. However, there were still very few cases in the junction of the two area or deep into wrong area, which indicates that these cases couldn't be distinguished well in the existing feature space. For the three baseline features, as shown in Fig. 14 (b), the aggregation of high risk and low risk cases and boundary between them were not obvious, and they tended to intermingle with each other in central area. It was difficult for classifiers to perform well in such a disorder feature space.

2) Classifier Selection Result: The performances of the different classifiers applied on training data, after hyperparameter tuning, are listed in Fig. 15. For the selected features, three optimal models with 93.75% accuracy were selected—including DT, GBDT and AdaBoost—all of which were DT-based classifiers partly because of the effect of using a wrapper method based on DT. For the baseline features, two optimal models with 75% accuracy were selected, including KNN and DT.

C. Performance of Classification

As shown in Fig. 16, the determined optimal models were finally tested on test set. Compared with a 68.75% accuracy for baseline model, three models with our single foot features had a large improvement in our dataset with an 87.5% accuracy.

The worse results of the baseline model might come from the unknown actual relative position of the feet and lower

feature dimension, which led to the omission of useful information. Our method using a single foot COP was more suitable for the shoe system and had better expansibility in multi-dimensions. Limited by the systematic error of BBS in fall risk identified [5], a 87.5% accuracy with confidence interval [63.98%:96.50%] was enough to indicate that the extracted multi-dimensional feature could comprehensively evaluate the difference between HR and LR groups, and the models based on these features have good generalization performance for HR and LR classification. Furthermore, high sensitivity (100%) meant the low misdiagnosis rate of our model and availability and practicality in real medical situation.

The results of the holdout validation had certain degrees of randomness and lacked repeatability, which partly depended on the size and partition of test set. To solve this problem, a feature space was used to assist in the result analysis. As can be seen from Fig. 14 (a), the triangle marks represent subjects in the test set, who were evenly distributed in each region of the feature space. Especially, those near the boundary of two groups who were easily confused were classified correctly; however, there were three bad cases in the feature space that went deeper into the wrong area and could not be correctly classified, including two LR and one HR. As can be seen from the red crosses in Fig. 14 (a), the only two false cases in the test result were from these three bad subjects. Therefore, if all of them had been excluded from test set, the accuracy was likely to improve further, which meant that no matter how the test set was divided, our assessment method could achieve an accuracy of approximately 87.5% or even better, and the result of holdout this time would be repeatable.

Existing models still had room for improvement for those cases who went deep into the wrong area in the feature space. Even though BBS were widely used as the standard method to identify fallers, it still suffered from the lack of reliability without 100% diagnostic accuracy [5]; therefore, a more systematic labeling method combining multiple evaluation criteria should be adopted to eliminate wrong label. Although the 90 gait cycles adopted in the study showed adequate performance to generalize long-term gait pattern among the elderly for daily monitoring, a more optimized step number could be further explored. Finally, some new features are required to distinguish these special individuals to further improve the accuracy and specificity.

IV. Conclusion

The aim of this study was to develop a fall risk assessment model for the elderly based on weak foot features, which was suitable for wearable plantar pressure acquisition system. To solve the sensitivity problem of single foot features and increase the significance of temporal consistency related features, a definition of "weak foot" was proposed and its effectiveness and necessity were verified in the statistical results. Based on the definition, 44 multi-dimensional GL features were extracted to comprehensively evaluate the difference between HR and LR groups; notably, the relationship between the fall risk and temporal inconsistency in the weak foot was discussed in our study, and a probability distribution method was also used to analyze the symmetry and temporal consistency of GLs. After the rigorous model selection procedure, an 87.5% accuracy on the test data and feature space demonstrated the effectiveness and reliability of our assessment model. In general, we believe that the method based on weak foot features with low misdiagnosis rate has the potential for long-term fall risk assessment in daily life.

TABLE III
List of Abbreviations

Abbreviation	Full name	Abbreviation	Full name
BBS	Berg Balance scale	LR	Low risk
SFRT	Sensor-based fall risk testing	AP	Anterior-posterior
COP	Center-of-pressure	ML	Medial-lateral
VGRF	Vertical ground reaction forces	1D	One-dimensional
GL	Gait line	2D	Two-dimensional
LogiR	Logistic regression	MIM	Mutual information maximization
KNN	k-Nearest neighbor	mRMR	Minimal-redundancy and maximal-relevance
SVM	Support vector machine	SFS	Sequential forward selection
DT	Decision tree	SBS	Sequential backward selection
RF	Random forest	LOSO	Leave-one-subject-out
GBDT	Gradient boosting decision tree	PPV	Positive predictive value
HR	High risk	NPV	Negative predictive value

Abbreviations

See Table III.

References

[1] P. J. Dobriansky, R. M. Suzman, and R. J. Hodes, "Why population aging matters—A global perspective," U.S. Dept. State, Washington, DC, USA, Tech. Rep. 07-6134, 2007, pp. 1–32. [Online]. Available: https://2001-2009.state.gov/g/oes/rls/or/81537.htm

[2] S. Liang, Y. Liu, G. Li, and G. Zhao, "Elderly fall risk prediction with plantar center of force using ConvLSTM algorithm," in *Proc. IEEE Int. Conf. Cyborg Bionic Syst. (CBS)*, Sep. 2019, pp. 36–41.

[3] S. S. Rao, "Prevention of falls in older patients," *Amer. Family Phys.*, vol. 72, no. 1, pp. 81–88, Jul. 2005.

[4] *WHO Global Report on Falls: Prevention in Older Age*, WHO, Geneva, Switzerland, vol. 15, no. 4, 2004.

[5] R. Sun and J. J. Sosnoff, "Novel sensing technology in fall risk assessment in older adults: A systematic review," *BMC Geriatrics*, vol. 18, no. 1, pp. 1–10, Dec. 2018.

[6] T. Shany, K. Wang, Y. Liu, N. H. Lovell, and S. J. Redmond, "Review: Are we stumbling in our quest to find the best predictor? Over-optimism in sensor-based models for predicting falls in older adults," *Healthcare Technol. Lett.*, vol. 2, no. 4, pp. 79–88, Aug. 2015.

[7] J. Howcroft, J. Kofman, and E. D. Lemaire, "Prospective fall-risk prediction models for older adults based on wearable sensors," *IEEE Trans. Neural Syst. Rehabil. Eng.*, vol. 25, no. 10, pp. 1812–1820, Oct. 2017.

[8] J. Howcroft, E. D. Lemaire, and J. Kofman, "Wearable-sensor-based classification models of faller status in older adults," *PLoS ONE*, vol. 11, no. 4, pp. 1–17, 2016.

[9] R. Rajagopalan, I. Litvan, and T.-P. Jung, "Fall prediction and prevention systems: Recent trends, challenges, and future research directions," *Sensors*, vol. 17, no. 11, pp. 1–17, 2017.

[10] D. Wang, J. Ouyang, P. Zhou, J. Yan, X. Xu, and L. Shu, "A novel low-cost wireless footwear system for monitoring diabetic foot patients," *IEEE Trans. Biomed. Circuits Syst.*, vol. 15, no. 1, pp. 43–54, Feb. 2021.

[11] D. Winter, "Human balance and posture control during standing and walking," *Gait Posture*, vol. 3, no. 4, pp. 193–214, Dec. 1995.

[12] A. L. Hof, M. G. J. Gazendam, and W. E. Sinke, "The condition for dynamic stability," *J. Biomech.*, vol. 38, no. 1, pp. 1–8, 2005.

[13] P. Di *et al.*, "Fall detection and prevention control using walking-aid cane robot," *IEEE/ASME Trans. Mechatronics*, vol. 21, no. 2, pp. 625–637, Apr. 2016.

[14] D. Lafond, H. Corriveau, and F. Prince, "Postural control mechanisms during quiet standing in patients with diabetic sensory neuropathy," *Diabetes Care*, vol. 27, no. 1, pp. 173–178, Jan. 2004.

[15] D. Toloza and M. Zequera, "Linear and non-linear methods for analysis center pressure and its application in diabetic peripheral neuropathy: A systematic review," in *Proc. 7th Latin Amer. Congr. Biomed. Eng. CLAIB*, in IFMBE Proceedings, vol. 60. Bucaramanga, Colombia, Oct. 2016, pp. 520–523. [Online]. Available: https://link.springer.com/chapter/10.1007/978-981-10-4086-3_179

[16] L. Rocchi, L. Chiari, and A. Cappello, "Feature selection of stabilometric parameters based on principal component analysis," *Med. Biol. Eng. Comput.*, vol. 42, no. 1, pp. 71–79, Jan. 2004.

[17] S. Morrison, S. R. Colberg, H. K. Parson, and A. I. Vinik, "Relation between risk of falling and postural sway complexity in diabetes," *Gait Posture*, vol. 35, no. 4, pp. 662–668, Apr. 2012.

[18] B. E. Maki, P. J. Holliday, and A. K. Topper, "A prospective study of postural balance and risk of falling in an ambulatory and independent elderly population," *J. Gerontol.*, vol. 49, no. 2, pp. M72–M84, Mar. 1994.

[19] C. Shin and T.-B. Ahn, "Asymmetric dynamic center-of-pressure in Parkinson's disease," *J. Neurolog. Sci.*, vol. 408, Jan. 2020, Art. no. 116559.

[20] A. Kalron and L. Frid, "The 'butterfly diagram': A gait marker for neurological and cerebellar impairment in people with multiple sclerosis," *J. Neurolog. Sci.*, vol. 358, nos. 1–2, pp. 92–100, Nov. 2015.

[21] M. N. Alam, A. Garg, T. T. K. Munia, R. Fazel-Rezai, and K. Tavakolian, "Vertical ground reaction force marker for Parkinson's disease," *PLoS ONE*, vol. 12, no. 5, May 2017, Art. no. e0175951.

[22] H. Bäzner, M. Oster, M. Daffertshofer, and M. Hennerici, "Assessment of gait in subcortical vascular encephalopathy by computerized analysis: A cross-sectional and longitudinal study," *J. Neurol.*, vol. 247, no. 11, pp. 841–849, Nov. 2000.

[23] K. Words, "Balance and symmetry measurements," *Phys. Ther.*, vol. 84, no. 2, pp. 128–136, 2004.

[24] A. Sant'Anna, A. Salarian, and N. Wickstrom, "A new measure of movement symmetry in early Parkinson's disease patients using symbolic processing of inertial sensor data," *IEEE Trans. Biomed. Eng.*, vol. 58, no. 7, pp. 2127–2135, Jul. 2011.

[25] P. Ren *et al.*, "Movement symmetry assessment by bilateral motion data fusion," *IEEE Trans. Biomed. Eng.*, vol. 66, no. 1, pp. 225–236, Jan. 2019.

[26] M. Siciliano, L. Trojano, G. Santangelo, R. De Micco, G. Tedeschi, and A. Tessitore, "Fatigue in Parkinson's disease: A systematic review and meta-analysis: Fatigue in Parkinson's disease," *Movement Disorders*, vol. 33, no. 11, pp. 1712–1723, Nov. 2018.

[27] K. Berg, S. Wood-Dauphine, J. I. Williams, and D. Gayton, "Measuring balance in the elderly: Preliminary development of an instrument," *Physiotherapy Canada*, vol. 41, no. 6, pp. 304–311, Nov. 1989.

[28] Y. Wu *et al.*, "Effect of active arm swing to local dynamic stability during walking," *Hum. Movement Sci.*, vol. 45, pp. 102–109, Feb. 2016.

[29] H. S. Yang, L. T. Atkins, D. B. Jensen, and C. R. James, "Effects of constrained arm swing on vertical center of mass displacement during walking," *Gait Posture*, vol. 42, no. 4, pp. 430–434, Oct. 2015.

[30] M. Ankerst, D. Keim, and H. Kriegel, "'Circle segments': A technique for visually exploring large multidimensional data sets," in *Proc. IEEE Vis. Hot Top. Sess.*, May 1996, pp. 5–8.

[31] P. Hoffman, G. Grinstein, K. Marx, I. Grosse, and E. Stanley, "DNA visual and analytic data mining," in *Proc. Vis.*, Oct. 1997, pp. 437–441.

[32] T. E. Prieto, J. B. Myklebust, R. G. Hoffmann, E. G. Lovett, and B. M. Myklebust, "Measures of postural steadiness: Differences between healthy young and elderly adults," *IEEE Trans. Biomed. Eng.*, vol. 43, no. 9, pp. 956–966, Sep. 1996.

[33] H. Sadeghi, P. Allard, F. Prince, and H. Labelle, "Symmetry and limb dominance in able-bodied gait: A review," *Gait Posture*, vol. 12, no. 1, pp. 34–45, Sep. 2000.

[34] D. D. Lewis, "Feature selection and feature extraction for text categorization," in *Proc. Speech Natural Lang., Workshop Held Harriman*, Oct. 1992, p. 212.

[35] M. A. Sulaiman and J. Labadin, "Feature selection based on mutual information," in *Proc. 9th Int. Conf. IT Asia (CITA)*, Aug. 2015, vol. 27, no. 8, pp. 1–6.

[36] T. Akiba, S. Sano, T. Yanase, T. Ohta, and M. Koyama, "Optuna: A next-generation hyperparameter optimization framework," in *Proc. 25th ACM SIGKDD Int. Conf. Knowl. Discovery Data Mining*, Jul. 2019, pp. 2623–2631.

[37] S. K. Stackhouse, J. E. Stevens, S. C. Lee, K. M. Pearce, L. Snyder-Mackler, and S. A. Binder-Macleod, "Maximum voluntary activation in nonfatigued and fatigued muscle of young and elderly individuals," *Phys. Therapy*, vol. 81, no. 5, pp. 1102–1109, May 2001.

[38] G. Zhang *et al.*, "Plantar pressure variability and asymmetry in elderly performing 60-minute treadmill brisk-walking: Paving the way towards fatigue-induced instability assessment using wearable in-shoe pressure sensors," *Sensors*, vol. 21, no. 9, p. 3217, May 2021.

[39] J. L. Helbostad, S. Leirfall, R. Moe-Nilssen, and O. Sletvold, "Physical fatigue affects gait characteristics in older persons," *J. Gerontol. A, Biol. Sci. Med. Sci.*, vol. 62, no. 9, pp. 1010–1015, Sep. 2007.

[40] J. A. García-Pérez, P. Pérez-Soriano, S. L. Belloch, Á. G. Lucas-Cuevas, and D. Sánchez-Zuriaga, "Effects of treadmill running and fatigue on impact acceleration in distance running," *Sports Biomech.*, vol. 13, no. 3, pp. 259–266, Jul. 2014.

[41] A. Katsiaras *et al.*, "Skeletal muscle fatigue, strength, and quality in the elderly: The health ABC study," *J. Appl. Physiol.*, vol. 99, no. 1, pp. 210–216, Jul. 2005.

[42] L. van der Maaten and G. Hinton, "Visualizing data using t-SNE," *J. Mach. Learn. Res.*, vol. 9, no. 11, pp. 1–48, 2008.